JOURNAL OF GUIDANCE, CONTROL, AND DYNAMICS
Vol. 30, No. 2, March–April 2007

Gauss's Variational Equation-Based Dynamics and Control for Formation Flying Spacecraft

Louis Breger* and Jonathan P. How†
Massachusetts Institute of Technology, Cambridge, Massachusetts 02139

DOI: 10.2514/1.22649

Formation flying is an enabling technology for many future space missions, and this paper presents several modeling and control extensions that would enhance the efficiency of many of these missions. In particular, a new linear time-varying form of the equations of relative motion is developed from Gauss's variational equations. These new equations of motion are further extended to account for the effects of J_2, and the linearizing assumptions are shown to be consistent with typical formation flying scenarios. It is then shown how these models can be used to initialize general formation configurations and can be embedded in an online, optimization-based, model predictive controller. A convex linear approach for initializing fuel-optimized partially J_2 invariant orbits is developed and compared with analytic approaches. All control methods are validated using a commercial numerical propagator. The simulation results illustrate that formation flying using this model predictive controller with J_2-modified Gauss's variational equations requires fuel use that is comparable to using unmodified Gauss's variational equations in simulations that do not include the J_2 effects.

Nomenclature

a	=	semimajor axis
b	=	semiminor axis
e	=	eccentricity
h	=	angular momentum
i	=	inclination
M	=	mean motion
n	=	orbit frequency
p	=	semilatus rectum
r	=	magnitude of radius vector
θ	=	argument of latitude
Ω	=	right ascension of the ascending node
ω	=	argument of perigee

I. Introduction

FORMATION flying of multiple spacecraft is an enabling technology for many future space science missions including enhanced stellar optical interferometers and virtual platforms for Earth observations [1,2]. Formation control objectives typically focus on controlling the relative states of the spacecraft, the dynamics of which can be captured using variants of Hill's and Lawden's equations for low-Earth-orbit (LEO) missions [3]. However, both of these approaches linearize the nonlinear relative spacecraft motions about a reference orbit, which is only valid for small separation distances of the satellites in the formation relative to the reference orbit radius. For larger separations, these equations of motion can no longer be used to cancel relative drift rates (initialization) or to accurately predict the effect of inputs (control) [4]. For example, the four spacecraft of the planned magnetospheric multiscale (MMS) mission [5] will be placed in a tetrahedron-shaped relative configuration with sides ranging between 10 and 1000 km, which far exceeds the separations for which Hill's and Lawden's models are valid for a full highly elliptic orbit (HEO) even with the correction terms introduced in [6]. Furthermore, these models do not accurately capture the effects of Earth's oblateness, which Schaub and Alfriend [7] showed can lead to very inefficient control designs. This paper develops a new linearized modeling approach that is valid for widely spaced formations in highly elliptic orbits, accurately captures the effects of Earth's gravity, and can be embedded in an optimization-based controller that is suitable for real-time calculations.

The relative dynamics used in this paper are based on a form of Gauss's variational equations (GVEs) that have been modified to include the effects of J_2. GVEs are convenient for specifying and controlling widely separated formations because they are linearized about orbital elements, which are expressed in a curvilinear frame in which large rectilinear distances can be captured by small element perturbations [8]. This bypasses the linearization error created by representing the entire formation in a single rectilinear frame, which was the approach used in [3]. The use of GVE dynamics as opposed to Hill's dynamics incurs the cost of computation associated with the use of multiple sets of time-varying equations of motion. Specifying a formation's relative geometry in terms of differential orbital elements is an exact approach that does not degrade for large spacecraft separations. However, the advantage of using GVEs for control could be reproduced by using a separate Lawden frame for each spacecraft in the formation while still using orbital element differences to represent the formation relative geometry. Given that a nonlinear transformation and rotation is required to switch between a local-vertical–local-horizontal (LVLH) frame and orbital element differences and that GVEs are already linearized in an orbital element frame, it is both simpler and computationally more efficient to use orbital element differences to specify the formation configuration and GVEs for control.

Many formation control approaches have used GVEs for nonlinear continuous control [9–11] and also for impulsive control [12,13]. This paper introduces a control law that generally does not fire continuously and, more importantly, makes explicit its objective to minimize fuel use, which is measured in ΔV in this paper. The control approach optimizes the effects of arbitrarily many inputs over a chosen planning horizon. Plans are regularly reoptimized, forming a closed-loop system [14]. By extending previous planning approaches [3,15] to use GVEs, we can optimize the plans for spacecraft in widely separated highly elliptic orbits. Results are presented to show that the GVE-based planning system is more fuel efficient than the four-impulse method in [12]. In addition control optimized online has the advantage of being capable of handling many types of constraints, such as limited thrust capability, sensor

Received 23 January 2006; revision received 10 April 2006; accepted for publication 18 April 2006.

*Research Assistant, Department of Aeronautics and Astronautics; lbreger@mit.edu.

†Associate Professor, Department of Aeronautics and Astronautics; jhow@mit.edu.

noise robustness, and error-box maintenance [3]. We also extend the *virtual center* approach to formation flying in [16] to GVEs and present a decentralized implementation of that algorithm.

A limitation of the orbital element approach in [15] is that it does not account for the effects of the J_2 disturbance, which impacted the closed-loop performance in full nonlinear simulations. This paper extends the use of the relative orbital elements in [15] to the J_2-modified relative state transition matrix in [17] and develops and evaluates several approaches for including the effects of thruster inputs. The resulting J_2-modified GVEs are used to form a set of linear parameter-varying dynamics that can be embedded in an optimization-based control system. The combination creates a controller that retains the advantages of the GVE-based controller in [15] but uses a more accurate dynamics model, thereby improving plan tracking and fuel efficiency. In particular, simulations are presented to show that the new controller in the presence of J_2 disturbances requires comparable levels of fuel to the approach in [15] when no J_2 disturbances are simulated in the model.

II. Relative Orbital Elements and Linearization Validity

GVEs are derived in [18] and are reproduced here for reference:

$$\frac{\mathrm{d}}{\mathrm{d}t}\begin{pmatrix} a \\ e \\ i \\ \Omega \\ \omega \\ M \end{pmatrix} = \begin{pmatrix} 0 \\ 0 \\ 0 \\ 0 \\ 0 \\ n \end{pmatrix} + \begin{pmatrix} \frac{2a^2 e \sin f}{h} & \frac{2a^2 p}{rh} & 0 \\ \frac{p \sin f}{h} & \frac{(p+r)\cos f + re}{h} & 0 \\ 0 & 0 & \frac{r\cos\theta}{h} \\ 0 & 0 & \frac{r\sin\theta}{h\sin i} \\ -\frac{p\cos f}{he} & \frac{(p+r)\sin f}{he} & -\frac{r\sin\theta\cos i}{h\sin i} \\ \frac{b(p\cos f - 2re)}{ahe} & -\frac{b(p+r)\sin f}{ahe} & 0 \end{pmatrix} \begin{pmatrix} \boldsymbol{u}_r \\ \boldsymbol{u}_\theta \\ \boldsymbol{u}_h \end{pmatrix} \tag{1}$$

where the state vector elements are a, e, i, Ω, ω, and M. The other terms in the variational expression are p, b, h, θ, r, and n. All units are in radians except for the semimajor axis and radius (in meters), the angular momentum (in kilogram meters squared per second), the orbit frequency (in 1/seconds), and the eccentricity (dimensionless). The input acceleration components $\boldsymbol{u}_r$, $\boldsymbol{u}_\theta$, and $\boldsymbol{u}_h$ are in the radial, in-track, and cross-track directions, respectively, of an LVLH frame centered on the satellite and have units of meters per second squared. Although the traditional Keplerian form of the orbital elements is used in this paper for conceptual clarity, later uses of transformations from [17,19] require a conversion to the nonsingular form described in those references. The form of the GVEs can be more compactly expressed as

$$\dot{\boldsymbol{e}} = A(\boldsymbol{e}) + B(\boldsymbol{e})\boldsymbol{u} \tag{2}$$

where $\boldsymbol{e}$ is the state vector in Eq. (1); $B(\boldsymbol{e})$ is the input effect matrix; $\boldsymbol{u}$ is the vector of thrust inputs in the radial, in-track, and cross-track directions; and $A(\boldsymbol{e}) = (0 \quad 0 \quad 0 \quad 0 \quad 0 \quad \sqrt{\mu/a^3})^T$, where μ is the gravitational parameter.

In a formation, the orbital element state of the ith satellite is denoted $\boldsymbol{e}_i$. The states of the vehicles in the formation can be specified by relative orbital elements by subtracting the state of an arbitrarily chosen spacecraft in the formation, which is designated as $\boldsymbol{e}_1$,

$$\delta\boldsymbol{e}_i = \boldsymbol{e}_i - \boldsymbol{e}_1 \tag{3}$$

For a desired orbit geometry, a set of desired relative elements, $\delta\boldsymbol{e}_{di}$ will specify the desired state $\boldsymbol{e}_{di}$ of each spacecraft in the formation. Approaches for choosing and coordinating the desired spacecraft states will be addressed in Secs. IV and VI.

$$\boldsymbol{e}_{di} = \boldsymbol{e}_1 + \delta\boldsymbol{e}_{di} \tag{4}$$

The state error for the ith spacecraft in the formation, ζ_i, is then defined as

$$\zeta_i = \boldsymbol{e}_i - \boldsymbol{e}_{di} = \delta\boldsymbol{e}_i - \delta\boldsymbol{e}_{di} \tag{5}$$

Note that the definition of state error given in Eq. (5) is independent of the choice of which spacecraft state is represented by $\boldsymbol{e}_1$. The form of GVEs in Eq. (1) is for perturbations of orbital elements. To reformulate these equations for perturbations of relative orbital elements [19], the GVEs for $\boldsymbol{e}_1$ and $\boldsymbol{e}_{di}$ are combined:

$$\dot{\zeta}_i = \dot{\boldsymbol{e}}_i - \dot{\boldsymbol{e}}_{di} = A(\boldsymbol{e}_i) - A(\boldsymbol{e}_{di}) + B(\boldsymbol{e}_i)\boldsymbol{u}_i \tag{6}$$

where the term $B(\boldsymbol{e}_{di})\boldsymbol{u}_{di}$ has been excluded because thrusting does not affect the desired state of the spacecraft. The unforced dynamics can be linearized by introducing the first-order approximation [19] (the subscript i is henceforth omitted for notational simplicity)

$$A(\boldsymbol{e}) - A(\boldsymbol{e}_d) \simeq \left.\frac{\partial A}{\partial \boldsymbol{e}}\right|_{\boldsymbol{e}_d} (\boldsymbol{e} - \boldsymbol{e}_d) = \left.\frac{\partial A}{\partial \boldsymbol{e}}\right|_{\boldsymbol{e}_d} \zeta \equiv A^*(\boldsymbol{e}_d)\zeta \tag{7}$$

where the matrix $A^*(\boldsymbol{e}_d)$ is all zeros except for the lower-leftmost element, which is $-3n/2a$, and where the sparsity of A^* arises from the sparsity of the A function in Eq. (2). With this approximation, the differential GVE expression in Eq. (6) can be rewritten as

$$\dot{\zeta} = A^*(\boldsymbol{e}_d)\zeta + B(\boldsymbol{e})\boldsymbol{u} = A^*(\boldsymbol{e}_d)\zeta + B(\boldsymbol{e}_d + \zeta)\boldsymbol{u} \tag{8}$$

In this case the control of the relative error state, ζ, is nonlinear because the control effect matrix B is a function of the state. Schaub and Junkins in [19] account for this nonlinearity in a continuous nonlinear control law that was shown to be asymptotically stable. The control approach developed in this section uses linearized dynamics to predict the effect of future control inputs. Linearizing the matrix B in Eq. (8) yields

$$\begin{aligned} \dot{\zeta} &\simeq A^*(\boldsymbol{e}_d)\zeta + \left(B(\boldsymbol{e}_d) + \left.\frac{\partial B}{\partial \boldsymbol{e}}\right|_{\boldsymbol{e}_d} \zeta\right)\boldsymbol{u} \\ &= A^*(\boldsymbol{e}_d)\zeta + B(\boldsymbol{e}_d)\boldsymbol{u} + [B^*(\boldsymbol{e}_d)]\zeta\boldsymbol{u} \end{aligned} \tag{9}$$

where the term $B^*(\boldsymbol{e}_d)$ is a third-rank tensor and the quantity $B^*(\boldsymbol{e}_d)\zeta$ is a matrix with the same dimensions as $B(\boldsymbol{e}_d)$. For convenience, define

$$\Delta B(\boldsymbol{e}_d, \zeta) \equiv B^*(\boldsymbol{e}_d)\zeta \tag{10}$$

resulting in the new state equation

$$\dot{\zeta} = A^*(\boldsymbol{e}_d)\zeta + (B(\boldsymbol{e}_d) + \Delta B(\boldsymbol{e}_d, \zeta))\boldsymbol{u} \tag{11}$$

Note that if ΔB is much smaller than $B(\boldsymbol{e}_d)$, then the first-order term can safely be ignored, yielding the approximate linearized dynamics

$$\dot{\zeta} = A^*(\boldsymbol{e}_d)\zeta + B(\boldsymbol{e}_d)\boldsymbol{u} \tag{12}$$

which can be controlled by any one of a variety of linear control techniques, including the model predictive controller discussed in Sec. IV.

The critical requirement for linear control and planning is that the term ΔB has a much smaller influence on the state dynamics than the term $B(\boldsymbol{e}_d)$. However, ΔB is a linear function of the state error ζ, which can be arbitrarily large. The amount of acceptable error due to linearization will be a function of the mission scenario, but the linearization assumption will typically be valid only for small values of the state error. It is reasonable to expect that the values of state error will be small because the linearization is only in separation between a spacecraft and its desired orbit. For a given desired orbit, a bound can be established numerically that indicates the state separation from an orbit where the dynamics linearization is valid. This section examines several example orbits that are representative of space missions that might occur in low and high Earth orbits. In

each case, the range of acceptable error is found to be large enough to accommodate expected mission performance requirements.

The magnitude of the acceptable error can be computed by comparing the induced norm of the difference between the control influence matrix at its desired state, $B(\boldsymbol{e}_d)$, and at the actual position of the spacecraft, $B(\boldsymbol{e})$. In Eq. (10), the first-order approximation of this term was defined as ΔB. In the following examples, ΔB_{true} is defined as

$$\Delta B(\boldsymbol{e}_d, \zeta)_{\text{true}} \equiv B(\boldsymbol{e}) - B(\boldsymbol{e}_d) = B(\boldsymbol{e}_d + \zeta) - B(\boldsymbol{e}_d) \tag{13}$$

and will be calculated numerically. The cutoff point of acceptable linearization error is when the norm of ΔB exceeds some (possibly mission dependent) fraction of the norm of $B(\boldsymbol{e}_d)$. To investigate this cutoff point, the following examples consider many random values of ζ in the set $||\zeta||_2 = r$ and calculate ΔB_{true}. The ΔB_{true} with the largest 2 norm will be used to test the validity of the linearization for a given r. This procedure is repeated for multiple r to find the largest $||\zeta||_2$ for which the linearization is considered valid. Other methods of examining the linearization error of B are possible, but the approach used in this paper was chosen because of its ease of implementation and consistent results for particular mission types.

A. Example: Low Earth Orbit

An example low Earth orbit is

$$\boldsymbol{e}_d = \begin{pmatrix} 6.9 \times 10^6 & 0.005 & 0.610865238 & 2\pi & \pi & 3.82376588 \end{pmatrix}^T \tag{14}$$

The matrix corresponding to $B(\boldsymbol{e}_d)$ is

$$B(\boldsymbol{e}_d) = \begin{pmatrix} -5.6794478 & 1808.6011 & 0 \\ -0.000082308780 & -0.00020502572 & 0 \\ 0 & 0 & 0.00010304404 \\ 0 & 0 & 0.00014406293 \\ 0.020528419 & -0.032987976 & -0.00011800944 \\ -0.020792326 & 0.032987564 & 0 \end{pmatrix} \tag{15}$$

where $||B(\boldsymbol{e}_d)||_2 = 1808.61$. The effect of perturbing $\boldsymbol{e}_d$ for a given norm bound on ζ is shown in Fig. 1. The plots show that a linearization validity cutoff of 0.01, i.e., $||\Delta B(\boldsymbol{e}_d, \zeta)_{\text{true}}||_2 \leq 0.01||B(\boldsymbol{e}_d)_{\text{true}}||_2$, can be achieved by ensuring that $||\zeta||_2 \leq 8.16 \times 10^{-3}$. This bound on ζ allows for orbital element perturbations that equate to rectilinear distances on the order of 25 km and velocities on the order of 40 m/s. Typical error-box sizes for LEO formation flying missions are 10–100 m in size [20], decidedly inside the linearization range of the orbit examined.

B. Example: Highly Elliptical Earth Orbit

One motivation for using GVEs as the linearized dynamics in a planner is recent interest in widely spaced highly elliptical orbits [5]. An orbit of this type is

$$\boldsymbol{e}_d = \begin{pmatrix} 4.20957 \times 10^7 & 0.818181 & 0.174532925 & 2\pi & 0 & \pi \end{pmatrix}^T \tag{16}$$

with

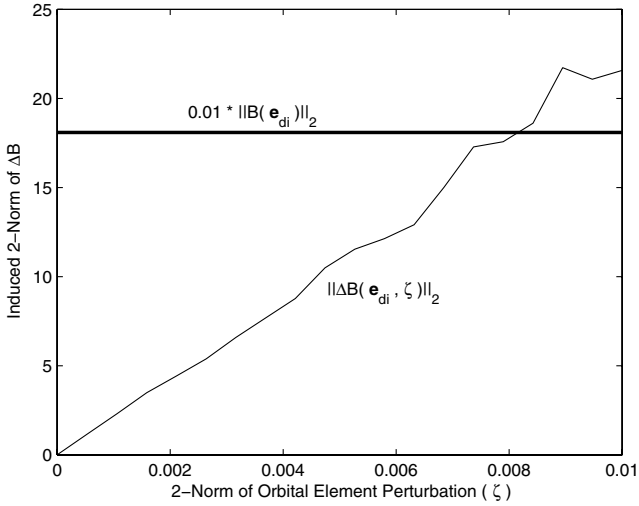

Fig. 1 Effect of orbital element perturbations on the ΔB_{true} matrix for the LEO example.

$$B(\boldsymbol{e}_d) = \begin{pmatrix} 4.767920 \times 10^{-12} & 8651.830 & 0 \\ 0 & -0.0003736926 & 0 \\ 0 & 0 & -0.001027650 \\ 0 & 0 & 0 \\ 0.0002283680 & 0 & 0 \\ -0.001313020 & 0 & 0 \end{pmatrix} \tag{17}$$

Repeating the same procedure used for the LEO case, it is determined from Fig. 2 that a 1% linearization validity cutoff can be achieved provided that $||\zeta||_2 \leq 3.66 \times 10^{-3}$. In this case, the bound on $||\zeta||_2$ corresponds to rectilinear distances of approximately 50 km and velocities of 2 m/s. As in the LEO case, these distances are far larger than expected error-box sizes. Because any planned trajectory would be expected to remain inside an error box at all times, the range of state errors in which the linearization is valid will not be exceeded. Unlike the LEO case, error boxes for widely separated missions, such as MMS, may be much larger than 10 m to a side, even approaching kilometers. The 1% cutoff ensures that error boxes of up to 5% of the distance between MMS satellites (1000 km during the most widely spaced phase of the mission) are acceptable [5].

Validating the linearization for additional reference orbits is a straightforward computational exercise. For example, repeating the

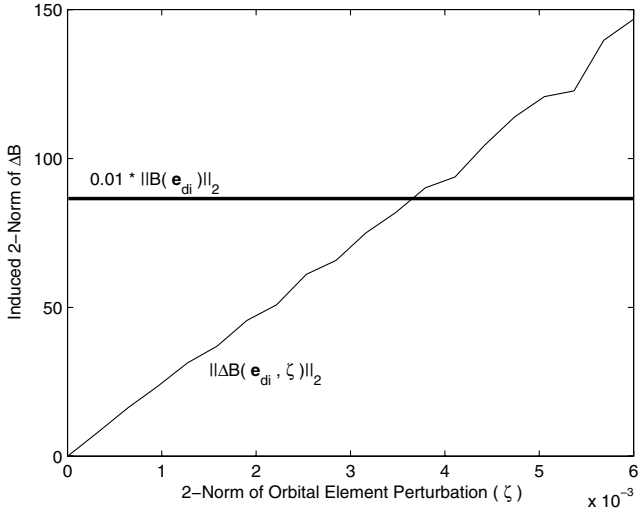

Fig. 2 Effect of orbital element perturbations on the ΔB_{true} matrix for the HEO example.

validation process for the LEO examples used in Sec. VI and the HEO examples used in the simulations in Sec. VII yielded valid ranges of separation that were far larger than the expected error-box sizes.

III. J_2-Modified Gauss's Variational Equations and Linearization Validity

Just as the GVEs in Eq. (2) express the motion of a Keplerian orbit, the equations of motion of the mean orbital element state vector $\boldsymbol{e}_m$ describe the average motion of an orbit influenced by Earth oblateness effects and are given by

$$\dot{\boldsymbol{e}}_m = \bar{A}(\boldsymbol{e}_m) + \frac{\partial \dot{\boldsymbol{e}}_m}{\partial \boldsymbol{u}}\boldsymbol{u} \tag{18}$$

where $\bar{A}$ is explicitly a function of the mean state and implicitly a function of J_2, see [19]. Although Eqs. (2) and (18) appear similar, there are some important differences. In particular, Eq. (2) describes the motion of a spacecraft's osculating orbit and is the form of the classical GVEs. Section II established that it is valid and effective to linearize the GVEs and use them for model predictive control. However, the GVEs incorporate neither the absolute nor the relative effects of J_2 on a satellite's orbit. Conversely, Eq. (18) describes the motion of an orbit in a set of mean orbital elements, where the secular effects of J_2 are incorporated and harmonics are removed. This form of the dynamics is useful for controlling the secular drift between satellites in a formation but does not describe the physical motion and has limited applicability for missions with high precision relative state constraints. Furthermore, Eq. (18) is nonlinear in terms of the relative state, which accurately captures the system dynamics but complicates the optimization of the control inputs. The following shows that, by using the linearized propagation and rotation matrices developed in [17], a linearized form of the equations of relative motion in Eq. (18) can be derived that incorporates the osculating effects of J_2, is linear parameter varying, and is valid for large spacecraft separations and reference orbit eccentricities.

The control influence matrix for mean element motion is derived using the transformation matrices between the mean and osculating motion. The following identity is used to define these transformations:

$$\frac{\partial \dot{\boldsymbol{e}}_m}{\partial \boldsymbol{u}} = \left(\frac{\partial \dot{\boldsymbol{e}}_m}{\partial \dot{\boldsymbol{e}}}\right)\left(\frac{\partial \dot{\boldsymbol{e}}}{\partial \boldsymbol{u}}\right) \tag{19}$$

From the appendix of [7], the relation between the mean orbital element state vector and the osculating orbital element state vector can be written as $\boldsymbol{e}_m = f(\boldsymbol{e})$, so that

$$\dot{\boldsymbol{e}}_m = \frac{\partial f(\boldsymbol{e})}{\partial \boldsymbol{e}}\dot{\boldsymbol{e}} \Rightarrow \frac{\partial \dot{\boldsymbol{e}}_m}{\partial \dot{\boldsymbol{e}}} = \frac{\partial f(\boldsymbol{e})}{\partial \boldsymbol{e}} \tag{20}$$

Substituting Eq. (20) and the B matrix from Eq. (2) into Eq. (19) gives

$$\frac{\partial \dot{\boldsymbol{e}}_m}{\partial \boldsymbol{u}} = \frac{\partial f(\boldsymbol{e})}{\partial \boldsymbol{e}}B(\boldsymbol{e}) \tag{21}$$

which yields the equations of motion of the mean orbit in terms of the osculating orbital state vector $\boldsymbol{e}$ (the mean elements may be considered a function of the osculating elements) and an input vector $\boldsymbol{u}$ as

$$\dot{\boldsymbol{e}}_m = \bar{A}(\boldsymbol{e}_m) + \frac{\partial f(\boldsymbol{e})}{\partial \boldsymbol{e}}B(\boldsymbol{e})\boldsymbol{u} \tag{22}$$

The actual mean orbit $\boldsymbol{e}_m$ is now defined in terms of a desired mean orbit $\boldsymbol{e}_{md}$ and a vector offset ζ_m

$$\boldsymbol{e}_m = \boldsymbol{e}_{md} + \zeta_m \tag{23}$$

Rearranging this expression and applying Eq. (18) gives

$$\dot{\boldsymbol{e}}_m - \dot{\boldsymbol{e}}_{md} = \dot{\zeta}_m = \bar{A}(\boldsymbol{e}_m) - \bar{A}(\boldsymbol{e}_{md}) + \frac{\partial \dot{\boldsymbol{e}}_m}{\partial \boldsymbol{u}}\boldsymbol{u} \tag{24}$$

where the term $(\partial \dot{\boldsymbol{e}}_{md}/\partial \boldsymbol{u})\boldsymbol{u}$ is omitted because the desired orbit is fixed and not subject to thrusting. Similar to the preceding section, the following linearization approximation can be made [19]:

$$\bar{A}(\boldsymbol{e}_m) - \bar{A}(\boldsymbol{e}_{md}) \approx \left.\frac{\partial \bar{A}}{\partial \boldsymbol{e}_m}\right|_{\boldsymbol{e}_{md}} \zeta_m \equiv \bar{A}^*(\boldsymbol{e}_{md})\zeta_m \tag{25}$$

which is then used to find the equations of motion of the mean element offset ζ_m,

$$\dot{\zeta}_m = \bar{A}^*(\boldsymbol{e}_{md})\zeta_m + \frac{\partial \dot{\boldsymbol{e}}_m}{\partial \boldsymbol{u}}\boldsymbol{u} \tag{26}$$

where the terms of the matrix function $\bar{A}^*$ are given in [21]. Equation (26) provides a linear description of the motion of the relative mean orbital elements. However, the mean orbit describes where the spacecraft is in an average sense, whereas the osculating orbits specify the actual position of spacecraft. Thus, to maximize the ability of the planner to exploit natural dynamics and operate with tight performance constraints, it is preferable to plan in terms of the osculating orbit. The approach in this paper uses a hybrid of the osculating and mean orbits to capture both the effects of J_2 and to plan in a way that accounts for the actual motion of the spacecraft. Having developed the relative dynamics in terms of the mean elements, we now convert to an osculating state.

Using the notation in Eq. (5), formation relative dynamics can be specified in terms of the osculating orbit $\boldsymbol{e}$, an osculating desired orbit $\boldsymbol{e}_d$, and an osculating orbital offset ζ between them. The mean elements are expressed as functions of the osculating elements by rearranging the state error form in Eq. (23). This is used to create a relative state and a linearized rotation matrix for the transition between the mean and osculating equations of relative motion.

Given that $\boldsymbol{e}_m = f(\boldsymbol{e})$ and $\boldsymbol{e}_{md} = f(\boldsymbol{e}_d)$, and then using Eq. (5), Eq. (23) can be rewritten as

$$\zeta_m = f(\boldsymbol{e}) - f(\boldsymbol{e}_d) \approx \left.\frac{\partial f(\boldsymbol{e})}{\partial \boldsymbol{e}}\right|_{\boldsymbol{e}_d} \zeta \tag{27}$$

by using the same linearization approach in [19]. Defining the matrix function D (available in [17]),

$$D(\boldsymbol{e}_d) \equiv \left.\frac{\partial f(\boldsymbol{e})}{\partial \boldsymbol{e}}\right|_{\boldsymbol{e}_d} \tag{28}$$

and substituting into Eq. (21) and then into Eq. (26) yields

$$\dot{\zeta}_m = \bar{A}^*(f(\boldsymbol{e}_d))\zeta_m + D(\boldsymbol{e})B(\boldsymbol{e})\boldsymbol{u} \tag{29}$$

This form of the relative equations of motion is nonlinear in terms of the osculating absolute state $\boldsymbol{e}$. Making the linearizing assumption (accuracy of the linear approximations are discussed later in this section)

$$D(\boldsymbol{e})B(\boldsymbol{e}) = D(\boldsymbol{e}_d + \zeta)B(\boldsymbol{e}_d + \zeta) \approx D(\boldsymbol{e}_d)B(\boldsymbol{e}_d) \tag{30}$$

allows the relative equations of motion to be rewritten as

$$\dot{\zeta}_m = \bar{A}^*(f(\boldsymbol{e}_d))\zeta_m + D(\boldsymbol{e}_d)B(\boldsymbol{e}_d)\boldsymbol{u} \tag{31}$$

which has a desired osculating orbit $\boldsymbol{e}_d$ and is linear in terms of the relative mean state ζ_m. The equations of motion in Eq. (31) are still not suited to control of the osculating relative orbit in the presence of J_2 because they describe the derivative of the mean state. The following section derives a form of discrete dynamics that use a relative osculating orbit as their state.

A. Extension to Discrete Time

To use Eq. (31) in an optimization-based controller of the type used in [15], it must first be discretized. Gim and Alfriend [17]

introduce the state transition matrix $\bar{\Phi}$, which is the discrete form of the continuous matrix $\bar{A}^*(f(\boldsymbol{e}_d))$, and is defined such that

$$\zeta_m(t_1) = \bar{\Phi}^*(\boldsymbol{e}_{md}(t_0), t_1, t_0)\zeta_m(t_0) \tag{32}$$

where t_0 and t_1 are the times of the initial and final states, respectively, and are provided as arguments to the state vectors. The analytic definition of the matrix $\bar{\Phi}^*$ (an implicit function of J_2 and a highly nonlinear function of the mean absolute elements) is included in the appendices of [17].

The dynamics in Eq. (31) can be formulated exclusively in terms of the osculating state. Using Eq. (27), define D^{-1} as

$$D^{-1}(\boldsymbol{e}_d) \equiv \left.\frac{\partial \boldsymbol{e}}{\partial f(\boldsymbol{e})}\right|_{\boldsymbol{e}_d} \tag{33}$$

Substituting Eqs. (28) and (33) into Eq. (32) yields

$$\zeta(t_1) \approx D^{-1}(\boldsymbol{e}_d(t_1))\bar{\Phi}^*(\boldsymbol{e}_{md}(t_0), t_1, t_0)D(\boldsymbol{e}_d(t_0))\zeta(t_0) \tag{34}$$

The analogous discrete form of the control influence matrix B on the osculating state is then given by

$$\Gamma(\boldsymbol{e}_d(t_0), t_1, t_0) = \int_{t_0}^{t_1} D^{-1}(\boldsymbol{e}_d(t_1))\bar{\Phi}^*(\boldsymbol{e}_{md}(\tau), t_1, \tau)D(\boldsymbol{e}_d(\tau))B(\boldsymbol{e}_d(\tau))\,\mathrm{d}\tau \tag{35}$$

Thus, combining Eqs. (32) and (35) yields the discrete time equations of motion

$$\zeta(t_1) \approx D^{-1}(\boldsymbol{e}_d(t_1))\bar{\Phi}^*(\boldsymbol{e}_{md}(t_0), t_1, t_0)D(\boldsymbol{e}_d(t_0))\zeta(t_0) + \Gamma(\boldsymbol{e}_d(t_0), t_1, t_0)\boldsymbol{u} \tag{36}$$

which are the linear parameter-varying discrete equations of motion for a relative osculating orbit in the presence of J_2.

B. Validity of the Linearization Approximations

In [6] Breger showed that the approximation $B(\boldsymbol{e}_d) \approx B(\boldsymbol{e}_d + \zeta)$, which is used to derive Eq. (36), is a sufficiently close approximation for levels of state error, ζ, that would normally be expected in spacecraft formation flying missions. To use Eq. (36) for linear control, it must also be shown that the linearized rotation and transition combination $D^{-1}(\boldsymbol{e}_d(t_1))\bar{\Phi}^*(\boldsymbol{e}_{md}(t_0), t_1, t_0)D(\boldsymbol{e}_d(t_0))$ remains a close approximation for expected values of ζ. In [17] Gim and Alfriend showed that this matrix has low linearization error for a wide range of reference orbit eccentricities and spacecraft formation baselines in excess of 10 km. By specifying the chief orbit in [17] as the desired spacecraft state, the transition matrices then allow a maximum state error of 10 km, which is much larger than the error that would be tolerated in most proposed spacecraft formation flying missions.

C. Calculating the Γ Matrix

The discrete control effect matrix is defined as a matrix integral in Eq. (35). One way to calculate this matrix is by computing its derivative and numerically integrating. However, in practice this is a computationally intensive approach that may not be consistent with real-time controller implementation. A number of alternate approaches exist. This subsection discusses several of those techniques and compares their accuracy and computation times.

1. *Continuous Integration*

The continuous integration method for getting the discrete input matrix Γ from time t_0 to time t_1 is

$$\Gamma_{\text{true}} = \int_{t_0}^{t_1} \left\{ D^{-1}(\boldsymbol{e}_d(t_1))\bar{\Phi}^*(\boldsymbol{e}_{md}(\tau), t_1, \tau)D(\boldsymbol{e}_d(\tau))M(\boldsymbol{e}_d(\tau)) \begin{bmatrix} 0_3 \\ I_3 \end{bmatrix} \right\} \mathrm{d}\tau \tag{37}$$

where

$$M\boldsymbol{x} = \delta\boldsymbol{e} \tag{38}$$

and the analytic form of M can be found in [19]. The vector $\boldsymbol{x}$ is in the LVLH coordinate system and has the form

$$\boldsymbol{x} = \begin{bmatrix} x & y & z & \dot{x} & \dot{y} & \dot{z} \end{bmatrix}^T \tag{39}$$

where the positions x, y, and z are in meters and the velocities $\dot{x}$, $\dot{y}$, and $\dot{z}$ are in meters per second. This approach should use no additional linearization assumptions beyond those in [17] because the inputs and their coupling effects are incorporated continuously. Although the outputs of the integration in Eq. (37) are very accurate, the approach itself requires significant computational effort (see Sec. III.C.5).

2. *Discretized Integration*

An approach to integrating Γ that is not as computationally intensive as the numerical integration is to approximate the integral in Eq. (37) discretely. This discrete approach introduces an additional time step Δt, which is the duration of each discrete term in the new approximate Γ. Conceptually, this approach is treating Γ as a series of smaller input effects, each based on a small time-invariant assumption. The discretized integration is

$$\Gamma_{\text{disc}} = \sum_{i=1}^{n} D^{-1}(\boldsymbol{e}_d(t_1))\bar{\Phi}^*(\boldsymbol{e}_{md}(t_0 + i\Delta t), t_1, t_0 + i\Delta t)D(\boldsymbol{e}_d(t_0 + i\Delta t))M(\boldsymbol{e}_d(t_0 + i\Delta t)) \begin{bmatrix} \frac{(\Delta t)^2}{2} I_3 \\ \Delta t I_3 \end{bmatrix} \tag{40}$$

where $(n+1)\Delta t = t_1 - t_0$. Here, a number of small double integrator assumptions are made, each one assuming that inputs of Δt seconds can safely ignore coupling effects.

3. *Rectilinear Dynamics Discretization*

Another approach to finding Γ is to use the discrete input matrix from a set of rectilinear equations of motion and to rotate it into relative orbital elements

$$\Gamma_{\text{rect}} = M(\boldsymbol{e}_d(t_0))\Gamma_{\text{LVLH}} \tag{41}$$

where Γ_{LVLH} is the discrete input matrix for a set of rectilinear equations of motion (e.g., inputs to a double integrator system, Hill's equations, or Lawden's equations). In Sec. V, an LVLH-based version of the approximated Γ matrix for Lawden's equations [22] is evaluated.

4. *Gauss's Variational Equation-Based Discretization*

An alternate approach to computing Γ is to use the continuous GVEs by taking the matrix exponential of the continuous matrix A^* from Eq. (7)

$$\Gamma_{\text{GVE}} = e^{A^*(t_1 - t_0)}B(\boldsymbol{e}_d(t_0)) \tag{42}$$

where B is the GVE matrix. This approach assumes the effects of J_2 on the input matrix are negligible.

5. *Validating* Γ

The continuous integration computation of Γ in Eq. (37) should not require any additional validation beyond the verification that the linearization assumptions in the component matrices D, $\bar{\Phi}^*$, and M are valid. To compare the matrices calculated using Eqs. (40–42),

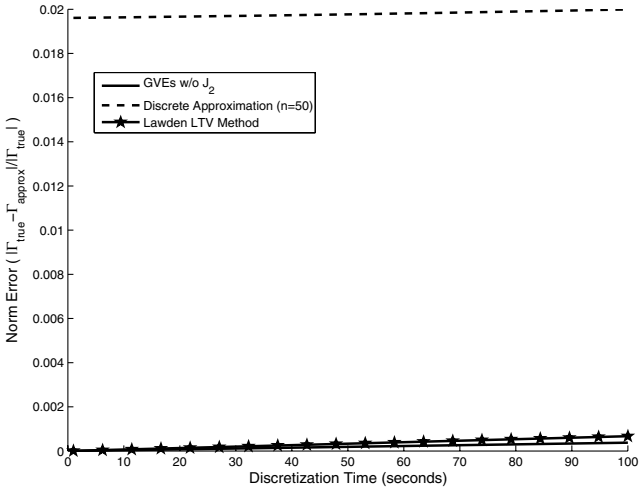

Fig. 3 Integrated vs approximated Γ for different discretization times in the LEO example.

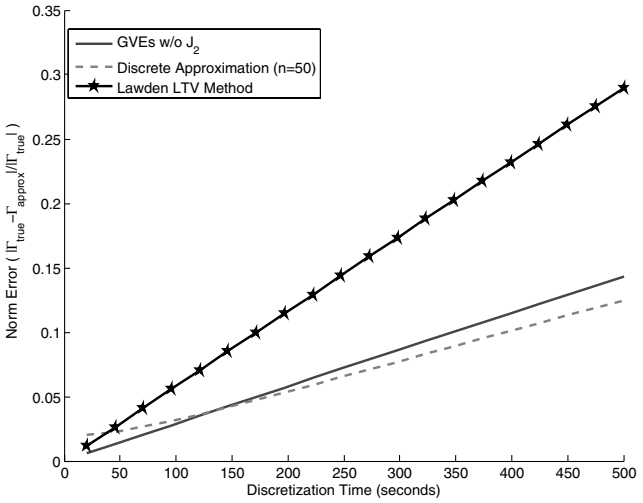

Fig. 4 Integrated vs approximated Γ for different discretization times in the HEO example.

their norm can be divided by that of the matrix generated using Eq. (37) (Γ_{true}) to find the normalized error

$$\epsilon_{\text{disc}} = \frac{||\Gamma_{\text{true}} - \Gamma_{\text{approx}}||_2}{||\Gamma_{\text{true}}||_2} \tag{43}$$

where Γ_{approx} is the Γ matrix computed using one of the approximate methods. If the error ϵ is kept sufficiently low (typical cutoff might be 0.01), then the approximate method would be considered valid. Figure 3 shows the values of ϵ computed for the three approximate methods (the continuous integration method is taken as the true Γ). Time step increments are used in Fig. 3, but an alternate validation method using true anomaly would be appropriate if steps of true anomaly are being used for plan implementation [23]. In the figure, "GVEs w/o J_2" refers to the ϵ for Γ_{GVE}, "Discrete Approximation ($n = 50$)" refers to the ϵ for Γ_{disc}, and "Lawden LTV Method" (where LTV stands for "linear time varying") refers to the ϵ for Γ_{rect}. The methods using Eqs. (41) and (42) are significantly more accurate than the discrete approximation. This difference can be corrected by refining the discretization time step; however, Table 1 shows that the discrete method using $n = 50$ already requires more computation time to evaluate. Hence, in the LEO example examined, the GVE- and Lawden-based approximations are both faster to compute and more accurate than the discrete approximation method for all discretization times. Although the methods in Eqs. (41) and (42) are marginally less accurate than the continuous integration, they are approximately 25 and 625 times as fast to compute, respectively.

Figure 4 shows how the evaluation of Γ using Eq. (42) degrades as the discretization time step is increased for the highly eccentric orbit ($e \approx 0.8$) case examined in Sec. II. In the figure, $\Delta\Gamma$ refers to the difference between the Γ calculated using Eqs. (40–42), respectively. For each time step, a series of $\Delta\Gamma$ matrices are evaluated, and the matrix with the largest induced 2 norm is used to represent the discretization error. Figure 4 indicates that the 86 s time step used in the simulations in Sec. VII is associated with just over 2% error between the Γ matrices for the GVE-based calculation method. As the time step grows larger, the discrete approach to computing Γ becomes marginally better than the other methods; however, it is still undesirable given that it is more than 250 times slower to compute than the method in Eq. (42).

Table 1 Average durations (in seconds) required to compute Γ matrices using various methods

Calculation method	Average computation time
Γ_{true}	1.02 s
Γ_{disc} ($n = 50$)	0.42 s
Γ_{rect}	0.041 s
Γ_{GVE}	0.0016 s

IV. Model Predictive Control Using Gauss's Variational Equations

In [3], Tillerson et al. showed that given a valid set of linearized dynamics and a desired trajectory, a model predictive controller for a spacecraft formation can be designed that allows for arbitrarily many convex terminal and intermediate state conditions, as well as sensor noise robustness requirements. This controller is implemented on each spacecraft in the formation, and it is using a linear programming formulation. The general form of the optimization performed by the controller is

$$\min ||U||_1 \text{ subject to } \mathbf{A}U \leq \boldsymbol{b} \tag{44}$$

where the matrix $\mathbf{A}$ and the vector $\boldsymbol{b}$ are formed based on the input dynamics and problem constraints and U is a vector of potential control input vectors

$$U = \begin{bmatrix} \boldsymbol{u}_i(1)^T & \boldsymbol{u}_i(2)^T & \cdots & \boldsymbol{u}_i(n-1)^T & \boldsymbol{u}_i(n)^T \end{bmatrix}^T \tag{45}$$

where each vector $\boldsymbol{u}_i(k)^T$ is the input for spacecraft i at step k for an n step plan.

To use the linearized GVE-based dynamics developed in Eq. (12) in the model predictive control (MPC) formulation, the dynamics can be discretized using a zero order hold assumption according to the procedure described in [24]. To use the linearized J_2-modified GVE-based dynamics developed in Eq. (31) in the MPC formulation, the discrete dynamics in Eq. (36) are used. Solutions to the optimization posed in Eq. (44) usually take the form of classical "bang-off-bang" optimal control laws. Figure 5 shows a typical plan to correct a small orbital element error. Note that although only two elements begin with errors, the optimized solution requires some elements to deviate from their desired states to minimize overall fuel use.

Solving the optimization in Eq. (44) with 1000 discretization steps and a terminal constraint has always required less than 0.05 s on a 3 GHz computer. Formulating the matrices used in the optimization has always taken under 10 s, far less than the 86 s discretization time step. The time required to formulate the problem will increase as the discretization step is made smaller and additional constraints are added. Although the computation numbers are very small, a more complicated formulation could still be implemented in a real-time system by specifying that thrusting not begin for several time steps into the plan. This will result in a plan that does not require action

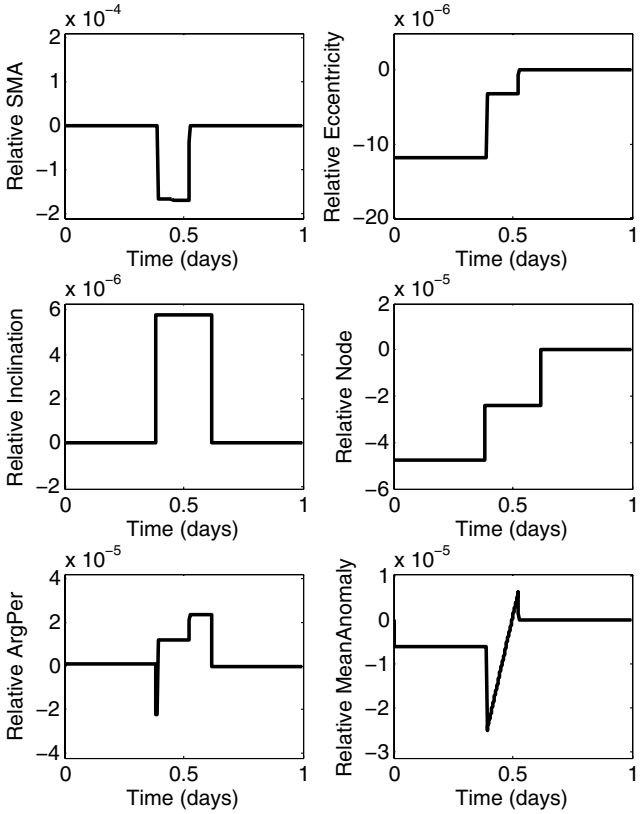

Fig. 5 Example plan generated using MPC with J_2-modified GVEs (lines indicate relative error).

until some specified time in the future when it is certain that the formulation and optimization will have been completed.

Figure 6 shows the error between a planned trajectory using the HEO example and the actual implemented trajectory when a trajectory is implemented without replanning (i.e., open loop). The majority of the orbit has near-perfect tracking, with error entering only near perigee, when nonlinearity effects are most significant. Note that the maximum trajectories following errors for each element in Fig. 6 are approximately $[7 \times 10^{-9},\ 8 \times 10^{-10},\ 1 \times 10^{-10},\ 1 \times 10^{-9},\ 1 \times 10^{-8},\ 2 \times 10^{-8}]$. This compares favorably with the maximums for the same trajectory following error using a controller based on the equations in Sec. II with no J_2 effects taken into account: $[1 \times 10^{-6}, 1.5 \times 10^{-8}, 4 \times 10^{-9}, 4 \times 10^{-8}, 8 \times 10^{-8}, 1 \times 10^{-7}]$. The maximum norm of the trajectory at any time is $||\zeta||_2 \approx 5 \times 10^{-5}$, which is significantly below 3.66×10^{-3}, the maximum norm of acceptable linearization error for this orbit, which was determined in Sec. II. Thus, it is valid to use the same linearized dynamics and controller to create a new plan from this terminal position. Repeatedly implementing new plans from a given initial error within the valid linearization range has always yielded terminal errors that were smaller and, hence, valid as initial conditions for replanning.

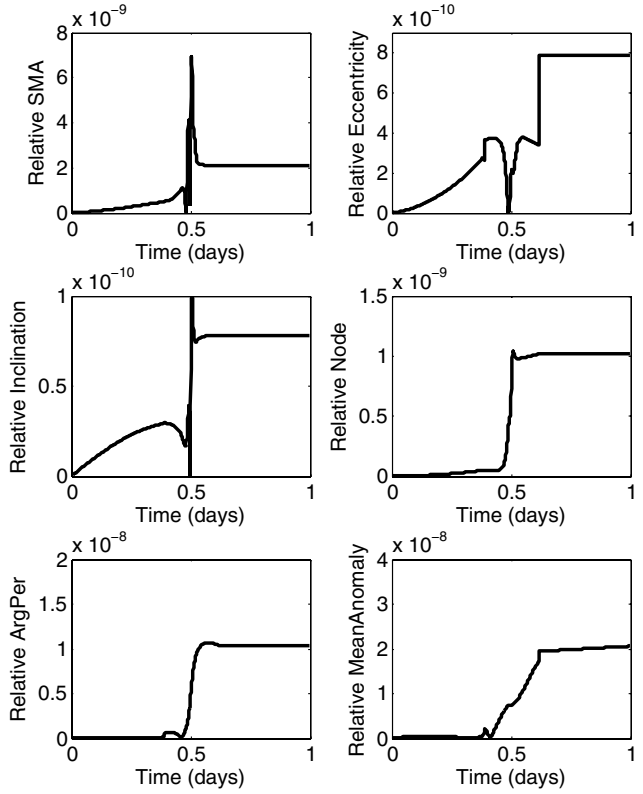

Fig. 6 Open-loop tracking (HEO). Lines indicate the difference between planned and implemented trajectories.

A. Error-Box Constraints Using Relative Orbital Elements

Several approaches have been developed to specify formation flying mission performance constraints. Generally, the goal of formation flying control is to keep the formation from "drifting apart" and to maintain some relative geometry. This requirement has been translated into maintaining orbits that have the same period and specifying desired relative states for spacecraft to follow. Both goals can be accomplished simultaneously by specifying relative desired points that have identical periodicity. Then to ensure that the spacecraft do not drift and that the formation geometry is maintained adequately, the control objective is to keep the spacecraft within some region around its desired point. This region is defined as a deadband in [25] and similarly as an error box in [3].

Maintaining a spacecraft within an error box has several advantages over tracking a desired point: it does not require fuel be used to correct minor deviations from the desired orbit, it better captures mission constraints that typically require only satellites to be in desired positions within some acceptable error, and it allows "breathing room" for the controller to account for modeling errors. In addition, the method of planning based on GVEs proposed in Sec. IV relies on the validity of the linearization analyzed in Sec. III, which degrades as the difference between the actual orbital element state and the orbital element state that has been linearized increases. If the error box used for a particular mission is smaller than the linearity range, which it typically would be (see Sec. II), the constraint that the spacecraft remain in the box provides an additional means of verifying that the linearity assumptions will be satisfied.

Several approaches can be taken to create an error box. Position error boxes are demonstrated in [3], which is a convenient bounding mechanism for a formation flying mission because it coincides well with science requirements on the accuracy of the formation geometry shape. When the formation geometry is specified in orbital elements, it is most convenient to use a six dimensional error box with bounds on each of the state elements. This approach, while simple and convenient for enforcing acceptable relative drift levels, does not map well into the position error-box constraints typical of previous performance specifications. To transition between LVLH error states, $\boldsymbol{x}$, and relative orbital element error states, ζ, a first-order rotation matrix $M(\boldsymbol{e}_d)$ is used [see Eq. (38)]. It is possible to enforce relative position and relative velocity error-box constraints using the $M(\boldsymbol{e}_d)$ matrix by formulating the optimization problem in Eq. (44) with constraints at every step k where it is desired that the spacecraft remain inside an error box

$$\boldsymbol{x}_{\min} \leq M^{-1}(\boldsymbol{e}_d)\zeta \leq \boldsymbol{x}_{\max} \tag{46}$$

where $\boldsymbol{x}_{\max}$ and $\boldsymbol{x}_{\min}$ denote opposing corners of the error box. To exclusively enforce a partial state error box (e.g., a position box), $M^{-1}(\boldsymbol{e}_d)$ can be premultiplied by an additional matrix H in Eq. (46) to retain only the desired components of the state.

B. Formation Flying: Coordination Using Gauss's Variational Equations

The model predictive controller described in Sec. IV is designed to be decentralized, with a fully independent controller being run on each spacecraft. The controller designs trajectories that will keep a spacecraft i inside an error box centered about the spacecraft's desired orbit, $\boldsymbol{e}_{di}$. In Sec. II, the desired orbits are defined with respect to the actual orbit of an arbitrary satellite in the formation, $\boldsymbol{e}_1$, using differential orbital element vectors, $\delta\boldsymbol{e}_{di}$, in the same manner used in [19]. In a system where initial conditions are chosen infrequently, it may be desirable to introduce additional coordination into the formation. When spacecraft each track desired states with no coordination, the control task is referred to as *formation keeping* [3]. Alternately, *formation flying* occurs when the spacecraft controllers collaborate to achieve formation-wide fuel minimization. This coordination can be achieved by calculating a central point that minimizes the overall weighted state error of each spacecraft in the formation. Approaches to implementing closed-loop coordination of this type are presented in [16,26]. The *virtual center* approach in [16] is a centralized calculation of the error-minimizing center based on fuel weighting and derived from measurements available through carrier-phase differential global positioning system (CDGPS) relative navigation of the type described in [27]. An equivalent approach can be used to find an error-minimizing reference orbit for a formation described in differential orbital elements.

Measurements from a CDGPS relative navigation system are assumed to be in the form of relative LVLH states [27], $\boldsymbol{x}_i$ [see Eq. (39)], for each satellite in the formation. The measurements will be relative to an arbitrary absolute satellite state, $\boldsymbol{e}_1$, in the formation, which is assumed to be at the origin of the LVLH frame. In addition to relative states, the global positioning system (GPS) sensors on each satellite can be expected to compute a less accurate estimate of the spacecraft's absolute state. Given an estimate of the absolute state in Earth centered inertial (ECI) coordinates, $\mathbf{X}_{\mathrm{ECI}_1}$ and the relative states $\boldsymbol{x}_i$, the differential states $\delta\boldsymbol{e}_i$ in Eq. (3) can be computed in several ways. The matrix $M(\boldsymbol{e}_1)$ in Eq. (38) could be computed and used to create a first-order approximation of the relative differential element states. However, an exact conversion can be calculated by forming estimates of the absolute states of each of the satellites based on their relative measurements

$$\mathbf{X}_{\mathrm{ECI}_i} = \mathbf{X}_{\mathrm{ECI}_1} + \boldsymbol{x}_i \tag{47}$$

The absolute states $\mathbf{X}_{\mathrm{ECI}_i}$ can be converted to Keplerian orbital elements, $\boldsymbol{e}_i$, of each satellite using a well-known procedure described in [21]. The relative measurements are then recovered in terms of differential orbital elements, $\delta\boldsymbol{e}_i$, using Eq. (3). Desired differential elements, $\delta\boldsymbol{e}_{dci}$, are then specified with respect to an unknown virtual center state, $\delta\boldsymbol{e}_c$, which is specified with respect to the absolute state $\boldsymbol{e}_1$. The error of spacecraft i with respect to the virtual center, ζ_{ci}, is given by [16]

$$\boldsymbol{e}_i - \delta\boldsymbol{e}_{dci} - \delta\boldsymbol{e}_c = \zeta_{ci} \tag{48}$$

which can be placed in the standard least-squares form $b_i - C_i\delta\boldsymbol{e}_c = \zeta_{ci}$, where $b_i = \boldsymbol{e}_i - \delta\boldsymbol{e}_{dci}$, C_i is a 6×6 identity matrix, and $\delta\boldsymbol{e}_c$ denotes the location of the virtual center with respect to $\boldsymbol{e}_1$ in differential orbital elements. By concatenating the b_i, C_i, and ζ_{ci} vectors for each spacecraft, the statement of error for the entire formation is written $b - C\delta\boldsymbol{e}_c = \zeta$, where $b = [b_1^T, \ldots, b_n^T]^T$, $C = [C_1, \ldots, C_n]^T$, and $\zeta = [\zeta_{c1}^T, \ldots, \zeta_{cn}^T]^T$. The solution that minimizes the error vectors globally in a weighted least-squares sense is

$$\delta\boldsymbol{e}_c = (C^T W C)^{-1} C^T W b \tag{49}$$

where W is a weighting matrix that can be used to bias the center location according to the fuel-use rates of different satellites in the formation, as well as to weight orbital elements individually based upon the amount of control required to alter them (obtainable from the GVEs for $\boldsymbol{e}_1$). This calculation can be decentralized and reduces the following iterative form [15]

$$\delta\boldsymbol{e}_{c_1} = b_1, \qquad \delta\boldsymbol{e}_{c_i} = \delta\boldsymbol{e}_{c_{i-1}} + \frac{w_i}{\bar{w}_{i-1} + w_i}\left(b_i - \delta\boldsymbol{e}_{c_{i-1}}\right) \tag{50}$$

where w_i is the weight of the ith estimate and $\bar{w}_i = w_1 + w_2 + \cdots + w_i$. In this formulation, a spacecraft i must pass its current state estimate, $\delta\boldsymbol{e}_{c_i}$, and the scalar $\bar{w}_i$ to the next spacecraft for a new estimate of the optimal center position to be formed. Using this method, the error-minimizing fuel-weighted virtual center can be known in one full cycle around a formation.

V. Comparison to Other Gauss's Variational Equation-Based Impulsive Control Schemes

The optimized controller developed in Sec. IV can be applied to a range of spacecraft control problems. This section uses that controller for the specific problem of correcting state error over a finite horizon to compare its performance and capabilities with other methods. GVEs have been used to design many Lyapunov and fixed impulse control systems [9,10,12,13,18]. Several research groups have proposed control laws for formation flying spacecraft that use GVEs to design impulsive thrusting maneuvers for orbit correction. A method of producing optimized impulsive plans for very low eccentricity orbits is presented in [28], but this approach does not extend to the higher eccentricities required for MMS missions. Another approach to using GVEs for formation control is to derive a continuous proportional-derivative controller satisfying a Lyapunov equation [9–11,19]. Control algorithms of this type have been shown to be asymptotically stable in most cases [11] but belong to a class of control systems that fire continuously. Continuous firing is generally not desirable for space missions because it is often disruptive to the science mission, it typically must be coupled with attitude maneuvers, and it expends fuel (nonreplenishable aboard a spacecraft) continuously.

The method of formation control in [13] is based on GVEs and uses a single corrective thrust computed using a nonlinear optimization. Although this method is guaranteed to find the optimal single-thrust correction for an arbitrary time period, it is not guaranteed (or likely) to find the optimal multiple-thrust correction. In addition, this approach is restricted to use in low Earth orbits and is only designed to correct errors in the semimajor axis, eccentricity, and inclination. An approach presented in [29] uses a pseudoinverse to the GVE control effect matrix to calculate a single corrective impulse. This approach is not guaranteed to be fuel optimal for any case and is not accurate for correcting position errors

Schaub and Alfriend [12] describe a controller that uses four impulses over the course of an orbit to correct arbitrary orbital element perturbations. Because of its more general applicability, this section will compare that approach to the MPC controller presented in Sec. IV. Both methods are designed to drive the elements of a state error ζ to zero over a fixed time interval. The four-impulse approach has not been presented in the context of performance criteria (e.g., trajectory or terminal error boxes, robustness to disturbances) or constraints (e.g., maximum thrust level), and so the comparisons in this section will use an MPC controller formulation that minimizes fuel use while driving the error state to zero in a fixed time and has no other constraints. In addition, for the purposes of comparison, no J_2 effects are used in either planning approach.

The algorithm in [12] can be summarized in four steps to be taken over the course of an orbit. When the argument of latitude is 0 or π radians, implement a velocity change (impulsive thrust), $\Delta v_{h_i} = [h/(r\cos\theta)]\Delta i$, in the cross-track direction of an LVLH frame centered on the spacecraft to cancel the inclination error component of ζ. When the argument of latitude is $\pi/2$ radians, implement a velocity change, $\Delta v_{h_\Omega} = [h\sin i/(r\sin\theta)]\Delta\Omega$ in the cross-track direction to cancel the ascending node error. At perigee and apogee, implement Δv_{r_p} and Δv_{r_a}, respectively, in the radial direction to cancel the argument of perigee and mean anomaly errors

$$\Delta v_{r_p} = -\frac{na}{4}\left[\frac{(1+e)^2}{\eta}(\Delta\omega + \Delta\Omega\cos i) + \Delta M\right] \tag{51}$$

$$\Delta v_{r_a} = \frac{na}{4}\left[\frac{(1-e)^2}{\eta}(\Delta\omega + \Delta\Omega\cos i) + \Delta M\right] \tag{52}$$

Also at perigee implement Δv_{θ_p} and at apogee implement Δv_{θ_a} in the in-track direction, to cancel the semimajor axis and eccentricity errors

$$\Delta v_{\theta_p} = \frac{na\eta}{4}\left(\frac{\Delta a}{a} + \frac{\Delta e}{1+e}\right) \tag{53}$$

$$\Delta v_{\theta_a} = \frac{na\eta}{4}\left(\frac{\Delta a}{a} - \frac{\Delta e}{1-e}\right) \tag{54}$$

Using the notation and the HEO reference orbit from Sec. II, the following example compares the MPC method with the control approach reviewed in this section. Note that in comparison to the MPC approach, the four-impulse method is very simple to implement. However, the two approaches have different rates of fuel use for identical tasks. For the state error

$$\zeta = \begin{pmatrix} 10^{-9} & 10^{-7} & 10^{-7} & 10^{-7} & 10^{-7} & 10^{-7} \end{pmatrix}^T \tag{55}$$

the four-impulse method requires 1.42 mm/s of fuel to correct the state error over the course of an orbit and the MPC method requires 0.549 mm/s of fuel. In this example, the model predictive controller was given a full orbit time horizon. However, the same control objective could have been achieved in less time, but using more fuel.

A series of 1000 orbital element state error vectors, ζ, was generated in which each perturbed element was a random number between $\pm 10^{-6}$. For each of the error vectors, both control methods were used to generate plans for eliminating the error. On average, the MPC maneuvers required only 51% of the fuel required by the four-impulse maneuver. Further controller comparisons are presented in Sec. VII.

VI. Fuel-Optimized Semi-J_2-Invariant Initial Conditions

Section IV presented a model predictive controller that can be used to create optimized plans for relative orbit control in the presence of J_2 disturbances. In a spacecraft formation, it is critically important both to conserve fuel when maneuvering and to maneuver to a state that will, over time, conserve fuel. The latter is an initial-condition (IC) problem, the specifications of which will depend on the unique requirements of a particular mission. However, in any spacecraft formation, a primary goal will be to prevent the vehicles from drifting apart, because that will typically end the mission. If the spacecraft in a formation tend to drift apart, then periodic maintenance maneuvers will be required to restore the formation. Initial conditions are called *invariant* if they eliminate drift, thereby allowing the spacecraft to maintain their relative orbits without expending fuel. In the context of this paper, invariance does not necessarily imply any form of relative boundedness at other points along the reference orbit, but this could be addressed by including additional error-box constraints to the optimization developed in this section.

For purely Keplerian orbits, invariance translates into a requirement that all spacecraft in a formation have the same semimajor axis. For example, this requirement was solved for analytically using Lawden's equations of motion in [30]. However, Earth oblateness effects (J_2) make orbits based on the Keplerian invariance solution drift apart. In fact, when the effects of J_2 are considered, very few perfectly invariant orbits exist. Hence, it is more common for a J_2 "invariant" orbit to instead be truly invariant only in several dimensions where it is possible to cancel the relative effects of J_2. Analytic conditions based on this partial invariance have been introduced [7,31]. The following presents an alternate approach that uses the dynamics in Sec. II and [17] in a convex linear optimization to find initial conditions that balance the objective of not drifting in the presence of relative J_2 effects against the objectives of minimizing the fuel use required to achieve these initial conditions and retaining a specified geometry for the formation.

To begin, specify that orbits are invariant if their relative orbital offset, $\delta\boldsymbol{e}$, in Eq. (5) remains unchanged over a period of time so that $\delta\boldsymbol{e}(t_1) \equiv \delta\boldsymbol{e}(t_2)$, where $t_2 - t_1$ is the duration of interest (typically an integer number of orbits). Then, using the state transition matrix from Eq. (34) gives the constraint

$$\delta\boldsymbol{e}(t_1) = \delta\boldsymbol{e}(t_2) = D^{-1}(\boldsymbol{e}(t_2))\bar{\Phi}^*(\boldsymbol{e}(t_1), t_2, t_1)D(\boldsymbol{e}(t_1))\delta\boldsymbol{e}(t_1) \tag{56}$$

Defining the matrix function $\bar{\Phi}^*_{Dk} \equiv D^{-1}(\boldsymbol{e}(t_{k+1}))\bar{\Phi}^*(\boldsymbol{e}(t_k), t_{k+1}, t_k)D(\boldsymbol{e}(t_k))$ gives the invariance condition

$$\delta\boldsymbol{e}(t_1) = \bar{\Phi}^*_{D1}\delta\boldsymbol{e}(t_1) \rightarrow (\bar{\Phi}^*_{D1} - I)\delta\boldsymbol{e}(t_1) = 0 \tag{57}$$

where I is a 6×6 identity matrix. As mentioned above, the resulting geometry of the no-drift (complete invariance) condition is too restrictive for many missions, but partially invariant conditions can be obtained by minimizing the weighted norm of the invariance condition

$$\min_{\delta\boldsymbol{e}(t_1)} ||W_d(\bar{\Phi}^*_{D1} - I)\delta\boldsymbol{e}(t_1)|| \tag{58}$$

where the weighting matrix W_d is introduced to extract states of interest to penalize particular types of drift. Note that if W_d is the matrix $M(\boldsymbol{e}(t))$ [see Eq. (37)], which rotates the differential osculating elements $\delta\boldsymbol{e}$ into an LVLH frame, then the elements of the LVLH state can be directly penalized (e.g., extracting only position states could penalize meters of drift). This enables the drift formulation to penalize the distance from the desired geometry in a Cartesian frame, as opposed to just using orbital elements. Penalizing true separation distance finds initial conditions that will maintain the formation shape, an important consideration for missions that require specific geometric configurations [5].

The overall problem statement then is, given a spacecraft at offset $\delta\boldsymbol{e}(t_0)$, design a control input sequence $U(\tau)$, $\tau \in [t_0, t_1]$, that generates a set of initial conditions at t_1 that balances the tradeoff between the ensuing drift by time t_2, the fuel cost of achieving these initial conditions, and the extent to which the formation geometry is maintained. The semi-invariant initial-condition optimization cost function is

$$\begin{aligned} C^* = \min_U \{ & Q_d ||W_d(\bar{\Phi}^*_{D1} - I)(\bar{\Phi}^*_{D0}\delta\boldsymbol{e}(t_0) + \hat{\Gamma}U)|| \\ & + Q_x ||W_x\hat{\Gamma}U|| + Q_u||U||\} \end{aligned} \tag{59}$$

where C^* is the optimal cost, W_x is a weighting matrix to specify the type of geometry penalty, Q_u is a weighting on fuel minimization, Q_x is a weighting on desired formation geometry, and Q_d is a weighting on drift. Using Eq. (56), $\delta\boldsymbol{e}(t_1) = \bar{\Phi}^*_{D0}\delta\boldsymbol{e}(t_0) + \hat{\Gamma}U$, where $\hat{\Gamma}$ is a row of convolved Γ matrices [see Eq. (35)] that propagate the effects of a vector of inputs (U) [see Eq. (45)] at each time step of the maneuver [3]

$$\begin{aligned} \hat{\Gamma} & \\ = & \begin{bmatrix} \tilde{\Phi}(n,1)\tilde{\Gamma}(0) & \tilde{\Phi}(n,2)\tilde{\Gamma}(1) & \cdots & \tilde{\Phi}(n,n-1)\tilde{\Gamma}(n-2) & \tilde{\Gamma}(n-1) \end{bmatrix} \end{aligned} \tag{60}$$

where $\tilde{\Phi}(k,j) \equiv D^{-1}(\boldsymbol{e}(kt_s))\bar{\Phi}^*(\boldsymbol{e}, kt_s, jt_s)D(\boldsymbol{e}(jt_s))$, $\tilde{\Gamma}(k) \equiv \Gamma(\boldsymbol{e}, (k+1)t_s, kt_s)$, and t_s is the discretization time step. The cost function uses the initial state of each spacecraft in the formation as the desired geometry, and so the geometry weighting penalizes deviations from the open-loop state propagation. Note that a simple modification to the cost function could separate the initial geometry from the desired geometry. The optimization in Eq. (59) can be easily implemented as a linear program if 1 norms are used, permitting efficient fast online solutions [32]. As expected, a sufficiently high weighting on invariance results in a minimizing control input U^*, where $\hat{\Gamma}U^* = -\bar{\Phi}^*_{D0}\delta\boldsymbol{e}(t_0)$. Alternately, a sufficiently high Q_x (with

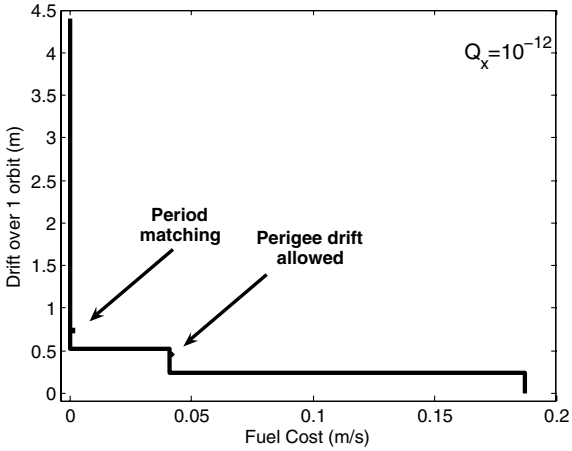

Fig. 7 Drift and fuel cost of a range of optimized initial conditions (LEO).

an identity matrix for W_x) results in $\hat{\Gamma}U^* = [0 \quad 0 \quad 0 \quad 0 \quad 0 \quad 0]^T$ because the inputs will all be zero to maintain the original geometry.

Figure 7 shows drift rates and fuel costs for a series of initial conditions generated by the optimization method with a half-orbit planning horizon as Q_d is changed. For this example, the 1-norm is used to penalize both drift and fuel use, and both W_d and W_x are set to the position rows of M to penalize only position drift and geometry separation. With a very low Q_d, Q_u will dominate, resulting in no control use. The zero drift point corresponds to high fuel use because it necessitates driving the spacecraft to nearly the same orbits. A range of possible optimized initial conditions lie in between those extrema. The high-drift unmodified initial conditions lie very close to the vertical drift axis but drop to just over 0.5 m of drift with a minimum of fuel use. Further drift reductions are possible, but at greater fuel cost. It is readily apparent from the graph that using additional ΔV will produce diminishing returns in terms of reducing drift.

Initial conditions generated by other J_2-invariant conditions should lie either on or above the optimized result. The ■ in Fig. 7 represents the initial condition based on the J_2-invariance condition in case 1 of [31], which requires no mean period drift. The point is nearly optimal for this example, but this is not guaranteed to be the case for other problems. The ◆ indicates the drift that occurs when using semi-invariant initial conditions that allow perigee drift [7]. In both specific cases, the partial invariance conditions allow for a range of possible initial conditions. Both analytic cases occur near the same drift levels as the initial conditions found by the optimizing approach. This indicates the optimized ICs may, in those cases, be meeting the same invariance criteria, while simultaneously finding ICs that minimize fuel use. The optimization-based approach enables the identification of a range of fuel-optimized initial conditions that can be used to better meet the requirements of a specific mission.

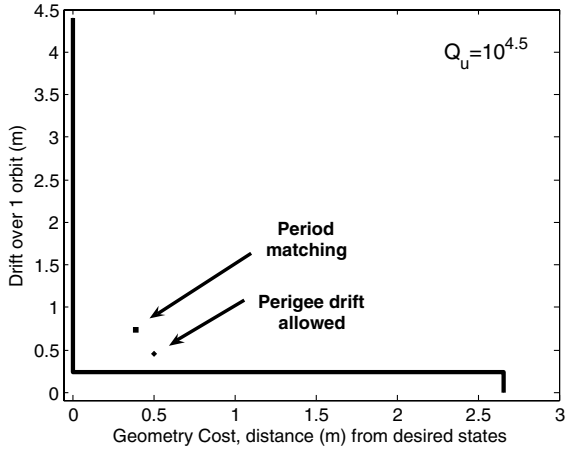

Fig. 8 Drift and geometry cost of a range of optimized initial conditions (LEO).

Figure 8 shows a number of optimizations of the same orbit and desired offset; however, in this case, both Q_x and Q_u are made significant whereas Q_d is varied. The figure shows the cost associated with changing the formation geometry ($||W_x\hat{\Gamma}U||_1$) versus the fuel cost ($||U||_1$). When Q_x is very high relative to Q_d, the optimized ICs, $\delta\boldsymbol{e}(t_1)$, are equivalent to the open-loop propagation of $\delta\boldsymbol{e}(t_0)$ (i.e., no fuel is used). This corresponds to 12 m of drift over an orbit. As Q_d is increased, the optimized ICs are farther from $\bar{\Phi}^*_{D0}\delta\boldsymbol{e}(t_0)$, but the resulting drift is lower because Q_d has a greater effect on the solution. The solution that achieves 0.25 m of drift with almost no geometry cost represents a compromise between the desired formation geometry and the drift resulting from the effects of relative J_2. At the cost of slightly repositioning the formation (velocity changes are not penalized in the W_d used for this example), the drift over an orbit has been reduced by over 4 m. When invariance dominates (the lower-right corner of the figure), the optimized initial conditions cancel almost all of the orbital offset $\delta\boldsymbol{e}$, indicating that geometry goals have been ignored.

VII. Formation Maintenance on a Highly Elliptic Mission

The control system described in Sec. IV was demonstrated on a segment of a mission similar to MMS, where four spacecraft create a regular tetrahedron geometry once per orbit to perform science observations. The orbits of the four spacecraft are widely separated and highly elliptical, presenting a challenge for many optimal formation specification and control approaches in the literature [23,30]. Using the tetrahedron initial-condition optimization approach in [15] and the model predictive approach in Sec. IV, the four spacecraft were controlled in a fully nonlinear simulation with Earth oblateness effects, atmospheric drag effects, and other realistic disturbances using a commercial orbit propagator [33]. The control objective in this simulation is to achieve a set of tetrahedron initial conditions once per day near the formation orbit apogee. The reference orbit for the formation is the highly eccentric orbit used in Sec. II.B.

To implement the MPC scheme in Sec. IV using the dynamics developed in Sec. III, the approximate rectilinear method of calculating Γ is used. The dynamics matrices Γ, $\bar{\Phi}$, and D are all functions of the desired orbital elements, which are parameter varying. To obtain accurate trajectories for the absolute desired orbital elements for the formation, they are integrated numerically with J_2 disturbance effects included and then used to generate the linear propagation matrices used in the optimization. The time step used in the simulation is 86 s, providing approximately 1000 discretization points in each day-long orbit. Constant time step duration was chosen to approximate typical flight computer operation, but plans with varying time steps can also be designed by planning in increments of true anomaly. Tillerson and How [23] discuss how these can be implemented. The planning horizon length for this simulation is one full day.

Figure 9 shows the rate at which fuel was used over the course of 1 week of formation flying. The formation fuel-use rate converges to approximately 12 mm/s per day ($\approx$1 orbit) for each satellite. Note that all previous simulations had to be limited to the case where the J_2 effects were disabled to ensure that the formation remained stable. In that case, for the same configuration, but without the effects of J_2 included in the controller dynamics or the simulation dynamics, the results showed an average ΔV of 11.5 mm/s per satellite per orbit. These nearly equivalent fuel-use rates for simulations with and without J_2 indicate that linearized modeling of J_2 effects in a controller of the type presented in Sec. IV is sufficient to prevent the disturbances from dominating fuel usage. The state error for one of the spacecraft in the formation is seen being driven to the origin in Fig. 10. Trajectories followed during this simulation fall within the range of acceptable state error determined for the linearizing assumptions used in Sec. III.

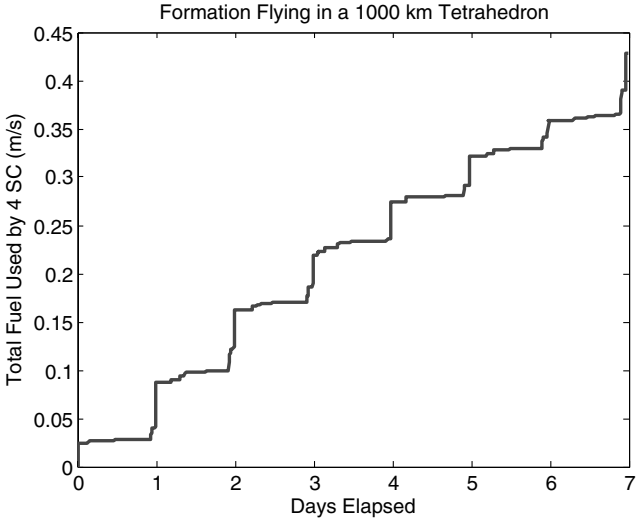

Fig. 9 Fuel cost of forming and maintaining a 1000 km tetrahedron formation (HEO).

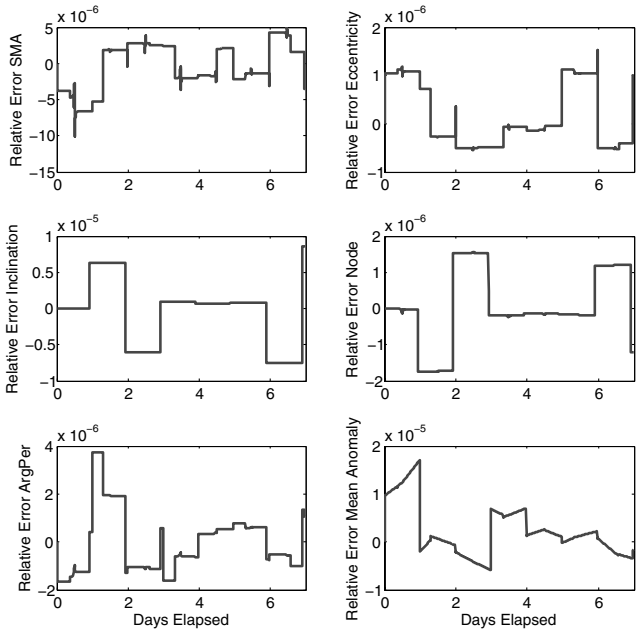

Fig. 10 Forming and maintaining a 1000 km tetrahedron formation in HEO (J_2 included).

VIII. Conclusion

A variant of GVEs that incorporates the effects of J_2 was used to derive a set of linearized relative dynamics of orbital motion and extend previous work on planning-based controllers. This choice of a linear parameter-varying (LPV) dynamics model to design the controller allows a compromise between simple, but inaccurate, linear models (e.g., Hill's equations) and high fidelity, but often difficult to control, nonlinear models. In particular, by accounting for J_2 disturbances in the dynamics, the planning controller can exploit these dynamics for improved fuel efficiency. The linearization assumptions used in the approach were shown to be valid for typical spacecraft error-box sizes. The LPV model was used in a model predictive controller, and the combination was shown to be more fuel efficient than a previously published technique. The overall control system (J_2-modified GVE-based dynamics embedded in the model predictive controller) was also used to specify and control a large (1000 km sides) tetrahedron-shaped formation in an MMS-like orbit for a period of 20 days using a commercial propagator with realistic disturbances. The results showed that the controller is reliable and that formation flying using this MPC with J_2-modified GVEs requires fuel use that is comparable to using unmodified GVEs in simulations that do not include the J_2 effects.

Acknowledgments

This work was funded under Cooperative Agreement NCC5-729 through the Goddard Space Flight Center Formation Flying NASA Research Announcement. Any opinions, findings, and conclusions or recommendations expressed in this material are those of the authors and do not necessarily reflect the views of the National Aeronautics and Space Administration. The authors would like to thank Terry Alfriend for his ideas and suggestions.

References

[1] Bauer, F. H., Hartman, K., Bristow, J., Weidow, D., How, J. P., and Busse, F., "Enabling Spacecraft Formation Flying Through Spaceborne GPS and Enhanced Autonomy Technologies," *ION-GPS '99, Proceedings of the 12th International Technical Meeting of the Satellite Division of the Institute of Navigation*, Institute of Navigation, Alexandria, VA, 1999, pp. 369–383; also Institute of Navigation Paper A01-27218 06-32.

[2] Leitner, J., Bauer, F., Folta, D., Moreau, M., Carpenter, R., and How, J. P., "Distributed Spacecraft Systems Develop New GPS Capabilities," *GPS World: Formation Flight in Space* [online journal], 1 Feb. 2002, p. 1, http://www.gpsworld.com/gpsworld/article/articleDetail.jsp?id=9518 [retrieved 15 Dec. 2005].

[3] Tillerson, M., Inalhan, G., and How, J. P., "Coordination and Control of Distributed Spacecraft Systems Using Convex Optimization Techniques," *International Journal of Robust and Nonlinear Control*, Vol. 12, Nos. 2–3, Feb.–Mar. 2002, pp. 207–242.

[4] Alfriend, K. T., Schaub, H., and Gim, D.-W., "Formation Flying: Accommodating Non-linearity and Eccentricity Perturbations," *12th AAS/AIAA Space Flight Mechanics Meeting*, American Astronautical Society Paper 02-184, Jan. 2002, pp. 1–20.

[5] Curtis, S., "The Magnetospheric Multiscale Mission Resolving Fundamental Processes in Space Plasmas," NASA TM2000-209883, Dec. 1999.

[6] Breger, L. S., Model Predictive Control for Formation Flying Spacecraft, S.M. Thesis, Dept. Aeronautics and Astronautics, Massachusetts Institute of Technology, Cambridge, MA, June 2004.

[7] Schaub, H., and Alfriend, K. T., "J_2 Invariant Relative Orbits for Spacecraft Formations," *Flight Mechanics Symposium*, NASA Paper 11, 2002.

[8] Junkins, J., Akella, M., and Alfriend, K. T., "Non-Gaussian Error Propagation in Orbital Mechanics," *Journal of the Astronautical Sciences*, Vol. 44, No. 4, 1996, pp. 541–563.

[9] Ilgen, M. R., "Low Thrust OTV Guidance using Lyapunov Optimal Feedback Control Techniques," *American Astronautical Society/AIAA Astrodynamics Specialist Conference*, American Astronautical Society Paper 93-680, Aug. 1993.

[10] Naasz, B., "Classical Element Feedback Control for Spacecraft Orbital Maneuvers,," S.M. Thesis, Dept. of Aerospace Engineering, Virginia Polytechnic Institute and State University, Blacksburg, VA, May 2002.

[11] Gurfil, P., "Control-Theoretic Analysis of Low-Thrust Orbital Transfer Using Orbital Elements," *Journal of Guidance, Control, and Dynamics*, Vol. 26, No. 6, Nov.–Dec. 2003, pp. 979–983.

[12] Schaub, H., and Alfriend, K., "Impulsive Feedback Control to Establish Specific Mean Orbit Elements of Spacecraft Formations," *Journal of Guidance, Control, and Dynamics*, Vol. 24, No. 4, July–Aug. 2001, pp. 739–745.

[13] Mishne, D., "Formation Control of LEO Satellites Subject to Drag Variations and J_2 Perturbations," *American Astronautical Society/AIAA Astrodynamics Specialist Conference*, AIAA Paper 2002-4430, Aug. 2002.

[14] Maciejowski, J. M., *Predictive Control with Constraints*, Prentice–Hall, Upper Saddle River, NJ, 2002.

[15] Breger, L. S., and How, J. P., "GVE-Based Dynamics and Control for Formation Flying Spacecraft," *2nd International Formation Flying Symposium*, Goddard Space Flight Center (NASA), Sept. 2004, pp. 1–12.

[16] Tillerson, M., Breger, L. S., and How, J. P., "Distributed Coordination and Control of Formation Flying Spacecraft," *Proceedings of American Control Conference*, IEEE Publications, Piscataway, NJ, June 2003, pp. 1740–1745.

[17] Gim, D. W., and Alfriend, K. T., "State Transition Matrix of Relative Motion for the Perturbed Noncircular Reference Orbit," *Journal of Guidance, Control, and Dynamics*, Vol. 26, No. 6, Nov.–Dec. 2003, pp. 956–971.
[18] Battin, R. H., *An Introduction to the Mathematics and Methods of Astrodynamics*, AIAA Education Series, AIAA, New York, 1987.
[19] Schaub, H., and Junkins, J. L., *Analytical Mechanics of Space Systems*, AIAA Education Series, AIAA, Reston, VA, 2003.
[20] Das, A., and Cobb, R., "TechSat 21—Space Missions Using Collaborating Constellations of Satellites," *Proceedings of the AIAA/Utah State University Annual Conference on Small Satellites*, Utah State University, Logan, UT, 1998, pp. 1–6; also Utah State University Paper A99-10826 01-20.
[21] Kaplan, M., *Modern Spacecraft Dynamics and Control*, Wiley, New York, 1976.
[22] Breger, L. S., Ferguson, P., How, J. P., Thomas, S., McLoughlin, T., and Campbell, M., "Distributed Control of Formation Flying Spacecraft Built on OA," *AIAA Guidance, Navigation, and Control Conference and Exhibit*, AIAA Paper 2003-5366, Aug. 2003.
[23] Tillerson, M., and How, J., "Formation Flying Control in Eccentric Orbits," *AIAA Guidance, Navigation, and Control Conference and Exhibit*, AIAA Paper 2001-4092, 2001.
[24] Franklin, G., Powell, J., and Workman, M., *Digital Control of Dynamic Systems*, 3rd ed., Addison Wesley Longman, Reading, MA, 1998.
[25] Carpenter, J. R., and Alfriend, K. T., "Navigation Accuracy Guidelines for Orbital Formation Flying," *AIAA Guidance, Navigation, and Control Conference and Exhibit*, AIAA Paper 2003-5443, Aug 11–14, 2003.
[26] Ren, W., and Beard, R., "Virtual Structure Based Spacecraft Formation Control with Formation Feedback," *AIAA Guidance, Navigation, and Control Conference and Exhibit*, AIAA Paper 2002-4963, Aug. 2002.
[27] Busse, F., How, J. P., Simpson, J., and Leitner, J., "PROJECT ORION-EMERALD: Carrier Differential GPS Techniques and Simulation for Low Earth Orbit Formation Flying," *IEEE Aerospace Conference*, Vol. 2, IEEE Publications, Piscataway, NJ, Mar. 2001, pp. 523–534.
[28] Carter, T. E., and Alvarez, S. A., "Quadratic-Based Computation of Four-Impulse Optimal Rendezvous near Circular Orbit," *Journal of Guidance, Control, and Dynamics*, Vol. 23, No. 1, Jan.–Feb. 2000, pp. 109–117.
[29] Mailhe, L., Schiff, C., and Hughes, S., "Formation Flying in Highly Elliptical Orbits: Initializing the Formation," *Proceedings of the International Symposium on Space Dynamics*, Centre National d'Etudes Spatiales Paper MS00/21, June 2000.
[30] Inalhan, G., Tillerson, M., and How, J. P., "Relative Dynamics & Control of Spacecraft Formations in Eccentric Orbits," *Journal of Guidance, Control, and Dynamics*, Vol. 25, No. 1, Jan.–Feb. 2002, pp. 48–59.
[31] Vadali, S. R., Alfriend, K. T., and Vaddi, S., "Hills Equations, Mean Orbital Elements, and Formation Flying of Satellites," American Astronautical Society Paper 00-258, March 2000.
[32] Bertsimas, D., and Tsitsiklas, J. N., *Introduction to Linear Optimization*, Athena Scientific, Belmont, MA, 1997.
[33] "FreeFlyer User's Guide," Ver. 4.0, A. I. Solutions, Inc., Lanham, MD, March 1999.